Available online at www.sciencedirect.com
SCIENCE DIRECT®
International Journal of Multiphase Flow 31 (2005) 996–1014
International Journal of Multiphase Flow
www.elsevier.com/locate/ijmulflow

History force on a sphere in a weak linear shear flow

L. Wakaba, S. Balachandar *

Department of Theoretical and Applied Mechanics, University of Illinois, Urbana-Champaign, IL 61801, USA

Received 25 January 2005; received in revised form 29 May 2005

Abstract

A numerical study of history forces acting on a spherical particle in a linear shear flow, over a range of finite *Re*, is presented. In each of the cases considered, the particle undergoes rapid acceleration from Re_1 to Re_2 over a short-time period. After acceleration, the particle is maintained at Re_2 in order to allow for clean extraction of drag and lift kernels. Good agreement is observed between current drag kernel results and previous investigations. Furthermore, ambient shear is found to have little influence on the drag kernel. The lift kernel is observed to be oscillatory, which translates to a non-monotonic change in lift force to the final steady state. In addition, strong dependence on the start and end conditions of acceleration is observed. Unlike drag, the lift history kernel scales linearly with Reynolds number and shear rate. This behavior is consistent with a short-time inviscid evolution. A simple expression for the lift history kernel is presented.

Keywords: History force; Lift history; Lift force; Shear-induced lift

1. Introduction

Unsteady force on a spherical particle has long been an area of interest, beginning with the works of Stokes (1851), Boussinesq (1885) and Basset (1888). The unsteady drag can be expressed as a sum of quasi-steady, added-mass, pressure gradient and history forces. In the Stokes limit, the

* Corresponding author. Tel.: +1 217 244 4371; fax: +1 217 244 9090.
E-mail address: s-bala@uiuc.edu (S. Balachandar).

0301-9322/$ - see front matter © 2005 Published by Elsevier Ltd.
doi:10.1016/j.ijmultiphaseflow.2005.05.009

history force decays as $t^{-1/2}$ in the time domain or correspondingly as $\omega^{-1/2}$ in the frequency domain (Landau and Lifshitz, 1959). It is now generally accepted that the $t^{-1/2}$ decay in the history force is valid only over a short-time and that the long-time decay is considerably faster (Sano, 1981; Mei et al., 1991; Mei and Adrian, 1992; Mei, 1993; Lovalenti and Brady, 1993a,b; Lawrence and Mei, 1995; Lovalenti and Brady, 1995; Chang and Maxey, 1994, 1995). The actual long-time decay rate shows variation even in the low Reynolds number limit. Depending on the nature of start and end conditions of acceleration/deceleration the long-time behavior of the history force shows either t^{-2} or t^{-1} decay and in some cases the history force decays even exponentially. At finite particle Reynolds numbers and at finite levels of acceleration, the short-time behavior still remains $t^{-1/2}$, but non-linearity further complicates the long-time behavior of the history force (Mei, 1993, 1994; Kim et al., 1998).

When the particle and ambient flow are in relative acceleration, the unsteady viscous effect of boundary layer development gives rise to the Basset history contribution to drag force. In the presence of ambient shear, the time-dependent boundary layer development will cease to be axisymmetric and a history contribution to lift force can be expected. The role of history contribution to drag force is well recognized (Michaelides, 1997), while in comparison the corresponding contribution to lift force is largely unexplored. The investigations of Legendre and Magnaudet (1998) and Asmolov and McLaughlin (1999) are of significance in this regard. Legendre and Magnaudet (1998) considered the transient behavior of lift force for the case of a spherical bubble suddenly introduced in a linear shear flow. Asmolov and McLaughlin (1999) studied the unsteady lift force on a sinusoidally oscillating sphere in a linear shear flow. Their singular perturbation analysis was limited to small oscillation amplitude and to $Re \ll Re_G^{1/2} \ll 1$, where Re and Re_G are Reynolds numbers based on relative velocity at the center of the particle and shear magnitude, respectively. With these assumptions, they obtained the unsteady lift force in the frequency domain, from which the history contribution can be extracted. In the high frequency limit their results are in agreement with those of Miyazaki et al. (1995), who considered the unsteady motion of a particle in an arbitrary linearly varying flow. At finite Reynolds numbers, evidence of the history effect in lift force comes from recent investigations of the free motion of a spherical particle in a linear shear flow by Bagchi and Balachandar (2002a). In these simulations, a particle was released from rest at $t = 0$ and as the particle accelerated in the ambient flow, its Reynolds number (based on relative velocity) monotonically decreased from its initial value. However, the lift force did not monotonically change from initial to final value. The quasi-steady component of lift force cannot account for this behavior and the non-monotonic evolution of the lift force can only be explained in terms of a history contribution. These finite Re computations were at large amplitude unsteadiness and thus they include a significant nonlinear effect.

Here, we will consider the unsteady rectilinear motion of a particle in a linear shear flow and the particle motion will be constrained to be parallel to the undisturbed streamlines. By carefully subjecting the particle to rapid acceleration over a very short period, the history contribution to lift force will be isolated and the lift history kernel (analogous to the Boussinesq–Basset history kernel for drag) will be extracted. Most interestingly, we observe the lift history kernel to be oscillatory, with an amplitude that decays over time. In particular, we observe that the changing sign of the kernel, its magnitude and the characteristic time of oscillation remain independent of the outer domain size. The non-monotonic behavior observed (Bagchi and Balachandar, 2002a) is related to this oscillatory behavior. As with drag force, the history kernel for lift is dependent on the

nature of acceleration or deceleration and is also influenced by non-linear effects associated with finite Re and finite amplitude acceleration. We however observe the lift history kernel to be different from the drag history kernel in several respects. Unlike the drag history kernel, which scales as $\sqrt{Re}$, we observe the lift history kernel to scale as Re. This fundamental difference in scaling can be explained in terms of the inviscid advection of vorticity in generating the transient lift force (Legendre and Magnaudet, 1998). The present simulations also provide information on the sensitivity of the drag history kernel to the presence of ambient shear.

2. Problem formulation

In a fixed laboratory frame of reference $(\mathbf{X}^*, t^*)$ the undisturbed ambient flow field (in absence of the particle) is given by

$$\mathbf{U}^*(\mathbf{X}^*) = G^* Y^* \mathbf{e}_X, \tag{1}$$

where "$*$" indicates dimensional variables and G^* is the dimensional shear rate of the flow. The instantaneous particle position $\mathbf{X}_\mathrm{p}^*(t^*)$ and velocity $\mathbf{V}_\mathrm{p}^*(t^*)$ allow for the following definition of instantaneous relative velocity at the location of the particle: $\mathbf{u}_r^*(t^*) = \mathbf{U}^*(\mathbf{X}_\mathrm{p}^*(t^*)) - \mathbf{V}_\mathrm{p}^*(t^*)$, where $\mathbf{U}^*(\mathbf{X}_\mathrm{p}^*(t^*))$ is the undisturbed ambient fluid velocity at the particle position. Non-dimensional shear rate (s) and Reynolds number (Re) are defined as $s = G^* d/|\mathbf{u}_r^*|$ and $Re = |\mathbf{u}_r^*| d/\nu$, where ν is the kinematic viscosity of the fluid. The Reynolds number based on shear magnitude can be defined as $Re_\mathrm{G} = G^* d^2/\nu = sRe$. It is convenient to adopt a non-inertial frame that is attached to the particle. In this frame the velocity perturbation ($\mathbf{u}$) to the undisturbed ambient shear flow satisfies the following non-dimensional equations:

$$\nabla \cdot \mathbf{u} = 0, \tag{2}$$

$$\frac{\partial(\mathbf{u} + \mathbf{V}_\mathrm{p})}{\partial t} + \mathbf{u} \cdot \nabla \mathbf{u} + \mathbf{U} \cdot \nabla \mathbf{u} + \mathbf{u} \cdot \nabla \mathbf{U} + \mathbf{V}_\mathrm{p} \cdot \nabla \mathbf{U} = -\nabla p + \frac{1}{Re_1} \nabla^2 \mathbf{u}, \tag{3}$$

where particle diameter and initial relative velocity are chosen as the length and velocity scales, and Re_1 is the initial Reynolds number based relative velocity.

In the above equations $\mathbf{U}$ and $\mathbf{V}_\mathrm{p}$ are the non-dimensional undisturbed ambient flow and particle velocity, respectively. The far field condition requires that $\mathbf{u} \to -\mathbf{V}_\mathrm{p}$ at large distances from the sphere and the no-slip and no-penetration conditions on the surface of the sphere require that $\mathbf{u}(|\mathbf{x}| = 1/2) = -\mathbf{U}(\mathbf{X}_\mathrm{p} + \mathbf{x})$. The total force on the sphere is obtained by integrating the pressure p and viscous stresses ($\tau_{r\theta}$ and $\tau_{r\phi}$) over the sphere surface:

$$\mathbf{F} = \int_S (-p\mathbf{e}_r + \tau_{r\theta}\mathbf{e}_\theta + \tau_{r\theta}\mathbf{e}_\phi)\, \mathrm{d}S \tag{4}$$

from which a dimensionless force coefficient vector is defined as

$$\mathbf{C}_\mathbf{F} = \frac{\mathbf{F}}{\frac{1}{2}\rho|\mathbf{u}_r^*|^2 \pi \left(\frac{d}{2}\right)^2}, \tag{5}$$

where ρ is the fluid density.

The governing equations are solved in spherical coordinates (r,θ,ϕ), using a pseudo-spectral method over the computational domain $\frac{1}{2} \leqslant r \leqslant R$, $0 \leqslant \theta \leqslant \pi$, and $0 \leqslant \phi \leqslant 2\pi$. The outer radius of the computational domain (R) is chosen to be 30 times the sphere radius. We have verified with additional simulations in a larger computational domain of twice the size that the results to be presented here are not sensitive to this choice of outer computational boundary. A Chebyshev collocation is used along the radial direction, while a Fourier collocation is used in the azimuthal (ϕ) direction. Variables in the tangential direction (θ) are defined over 0 to π and are expressed in terms of either even or odd Fourier modes, such that the appropriate "pole parity" conditions are satisfied. Grid stretching is used in both radial and tangential directions, in order to enhance resolution in the shear layers and in the sphere wake. A uniform distribution of collocation points is used along the periodic, azimuthal direction. A typical grid resolution used in the present simulations is $N_r \times N_\theta \times N_\phi = 81 \times 80 \times 32$. The flow field is advanced in time through a time-split scheme that separates the solution procedure of the governing equations into an advection–diffusion step followed by a pressure correction step. At the inflow section of the outer boundary, the far field condition ($\mathbf{u} \to -\mathbf{V}_\mathrm{p}$) is applied, while at the outflow section a non-reflecting buffer domain technique (Mittal and Balachandar, 1996) is implemented. For further details on the numerical methodology see Bagchi and Balachandar (2002a).

2.1. Extraction of history kernel

The unsteady drag on a spherical particle, in a spatially uniform ambient flow, can be expressed in dimensional terms as (Mei, 1994):

$$F^*_\mathrm{D} = 3\pi\mu d u^*_r \phi + \frac{1}{2} m_\mathrm{f} \frac{\mathrm{d}u^*_r}{\mathrm{d}t^*} + m_\mathrm{f} \frac{\mathrm{D}U^*}{\mathrm{D}t^*} + 3\pi\mu d \int_{-\infty}^{t^*} K_\mathrm{D}(t^* - \tau^*) \frac{\mathrm{d}u^*_r}{\mathrm{d}\tau^*} \mathrm{d}\tau^*, \tag{6}$$

where m_f is the mass of fluid displaced by the particle. In this case, $u^*_r(t^*)$ denotes the instantaneous relative velocity in the direction of ambient flow. The first term on the right is the quasi-steady drag and it includes the finite Reynolds number correction: $\phi = (1 + 0.15Re^{0.687})$. Generally, in a non-uniform ambient flow, further correction may be needed for the quasi-steady drag (Bagchi and Balachandar, 2002c,b), however this correction is quite small and can be neglected in the case of a shear flow (Bagchi and Balachandar, 2002a; Kurose and Komori, 1999). The second term on the right is the added-mass force and the third term is the pressure-gradient force. The last term is the history integral and it accounts for the unsteady viscous effect. The following history kernel was proposed by Mei and Adrian (1992) and Mei (1994):

$$K_\mathrm{D}(t^* - \tau^*) = \left\{ \left[\frac{4\pi(t^* - \tau^*)\nu}{d^2} \right]^{1/4} + \left[\frac{\pi |u^*_r|^3 (t^* - \tau^*)^2}{d\nu f_\mathrm{H}^3} \right]^{1/2} \right\}^{-2}, \tag{7}$$

where $f_\mathrm{H} = 0.75 + 0.105Re$. The above kernel will be referred to as K_Mei in further discussions. For sufficiently short time, the above history kernel reduces to the classic Boussinesq–Basset kernel (will be referred as the BB kernel or K_BB):

$$K_\mathrm{D}(t^* - \tau^*) = \left[\frac{4\pi(t^* - \tau^*)\nu}{d^2} \right]^{-1/2}. \tag{8}$$

In the present context of a linear shear flow, we limit the particle motion to be only along the flow direction and thus the relative velocity is constrained to be along X. For the evaluation of the history kernel, we consider the case where, for $t < 0$, the motion of the particle is initially steady at a relative velocity of u_{r1}, and the particle is suddenly accelerated after $t = 0$ such that the relative velocity rapidly reaches u_{r2}. After this short period of rapid acceleration, the particle maintains a steady motion at this new relative velocity. Correspondingly, the Reynolds number based on relative velocity changes from Re_1 to Re_2. At all times the particle sees the same constant linear ambient shear and only the relative velocity is varied. Thus, Reynolds number based on shear (Re_G) remains independent of time, while the non-dimensional shear rate varies from $s_1 = Re_G/Re_1$ to $s_2 = Re_G/Re_2$. Once the particle reaches its final steady motion, the added-mass and pressure-gradient forces are identically zero and the quasi-steady force remains time independent. Thus, the history contribution to drag can be separated from the total drag force. For the special case where the jump from Re_1 to Re_2 occurs instantaneously at $t = 0$ (corresponding to a step function change in relative velocity), the history kernel can be expressed as (see Appendix A):

$$K_D(t) = \frac{1}{24}\frac{Re_2^2}{(Re_2 - Re_1)}(C_D(t) - C_D(\infty)). \tag{9}$$

In numerical computations, the step change in relative velocity needs to be approximated. Here, we replace the delta function acceleration by a steady acceleration of $(u_{r2} - u_{r1})/t_s$ that extends over a short-time span, $0 \leqslant t \leqslant t_s$ (see Fig. 1(a)).

The duration of acceleration, t_s, can be set equal to the time step of the time advancement scheme (Δt). But for increased computational accuracy, the acceleration is extended over several time steps and thus the relative velocity is linearly ramped from the start to the end value. The final history kernel result must be insensitive to the precise value of the two numerical parameters, t_s and Δt, and this will be verified below. With the finite duration of acceleration, a simple approximation to the history integral will lead to an improved estimation of the history kernel from the computed drag coefficient (see Appendix A).

The above analysis can be extended for lift force as well. In the post-acceleration phase (for $t > t_s$), the lift force has contributions from only the quasi-steady part and the history term, i.e., $F_L^* = F_{L,QS}^* + F_{L,H}^*$. The history contribution to the lift force will be expressed as a time integral (similar to that for drag):

$$F_{L,H}^*(t^*) = 3\pi\mu d\int_{-\infty}^{t^*} K_L(t^* - \tau^*)\frac{du_r^*}{d\tau^*}\,d\tau^*, \tag{10}$$

where K_L is the lift history kernel. From the computed time evolution of drag and lift coefficients, the corresponding history kernels can be extracted as follows (see Appendix A):

$$\begin{aligned} K_D(t) &\approx \frac{1}{24}\frac{Re_2^2}{(Re_2 - Re_1)}\left(C_D\left(t + \frac{t_s}{2}\right) - C_D(\infty)\right) \\ K_L(t) &\approx \frac{1}{24}\frac{Re_2^2}{(Re_2 - Re_1)}\left(C_L\left(t + \frac{t_s}{2}\right) - C_L(\infty)\right). \end{aligned} \tag{11}$$

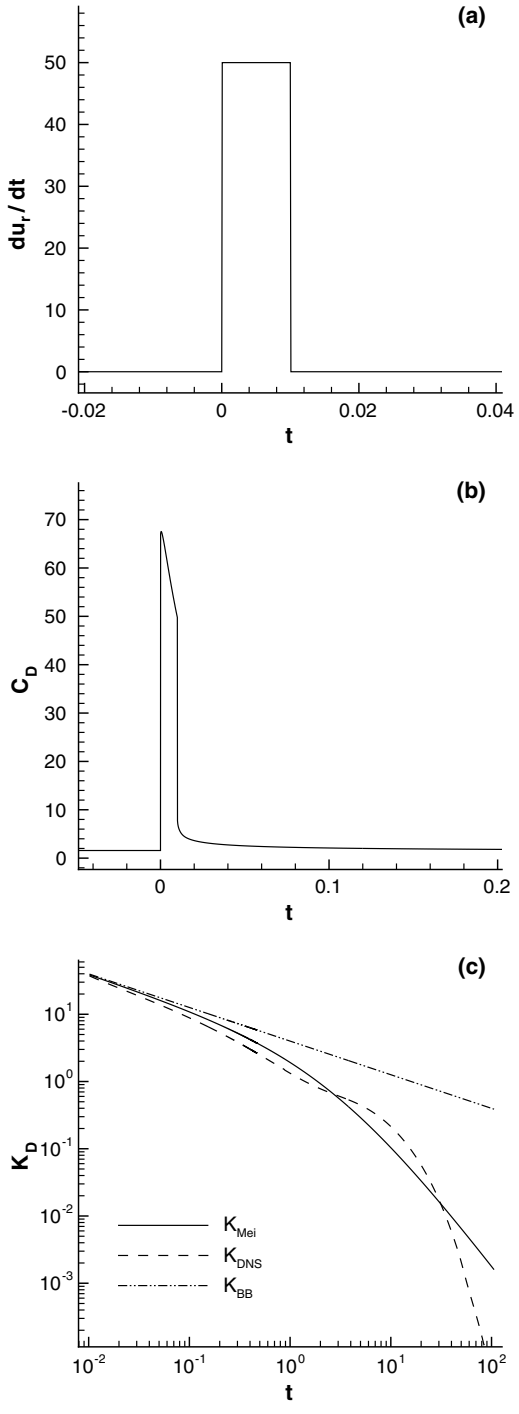

Fig. 1. Particle motion in a uniform flow with step change in relative velocity from $Re_1 = 50$ to $Re_2 = 62.5$. (a) Time history of du_r/dt. (b) Time evolution of drag coefficient. (c) Comparison of drag history kernel obtained from DNS with corresponding kernels by Mei (1993) and Boussinesq and Basset.

3. Results

3.1. Uniform ambient flow

We first consider the case of a particle undergoing a step change in its relative velocity, in a uniform ambient flow. In this example, the Reynolds number (based on relative velocity) is rapidly increased from its initial value of 50 to a steady final value of 62.5. Fig. 1(a) shows a constant relative acceleration of non-dimensional magnitude 50 over a short duration of $t_s = 1 \times 10^{-2}$. Fig. 1(b) shows the computed time evolution of the drag coefficient. The drag coefficient remains steady for $t < 0$ and undergoes sudden jumps at the beginning and end of acceleration, due to added-mass and pressure-gradient forces. The near linear decrease in C_D during the period of acceleration is due to the increase in relative velocity (see (5)). After acceleration, C_D slowly decays over a long period to approach a steady state corresponding to the final relative velocity. Fig. 1(c) shows the history kernel extracted using (11) from the computed drag coefficient shown in frame (b). Also shown for comparison are K_{Mei} and K_{BB}. The different kernels are in agreement for a very short-time period. The history kernel proposed by Mei (1994) exhibits the expected faster t^{-2} decay for long time. The decay of the computed history kernel shows a slow down at some intermediate time, but eventually increases beyond t^{-2}. The behavior seen in Fig. 1(c) is in complete agreement with the numerical results of Mei (1993).

The non-dimensional time step in the above simulation was maintained small ($\Delta t = 1 \times 10^{-4}$) at the beginning, in order to adequately resolve the details of the flow during and shortly after the rapid acceleration. The time step was later increased to $\Delta t = 1 \times 10^{-3}$, which was well within the stability limits of the code. The effect of time step was investigated by varying Δt. Fig. 2(a) shows the drag history kernel obtained from three different time steps and it is clear that the results are independent of the time step. The effect of finite duration of acceleration was also investigated by varying t_s from 1×10^{-2} to 2.5×10^{-3} and the corresponding history kernels shown in Fig. 2(b) demonstrate the independence of results to details of t_s. Further results to be presented are similarly verified to be well converged in terms of Δt and t_s.

The requirement of spatial resolution has been well tested in earlier works for both uniform and sheared ambient flows (Bagchi and Balachandar, 2002a,c). In the present simulations, the entire computational domain is very well resolved. In the extraction of the history kernel, additional attention must be paid to the placement of the outer boundary. Mei (1993) commented that a very large computational domain may be required to accurately address the very long-time behavior of the history kernel. Kim et al. (1998), however, found the placement of the outer boundary to have less of an influence. In any case, here we will limit our attention to the behavior of the drag and lift history kernels over short and intermediate times when the viscous change to the wake is well represented by the computational domain.

3.2. Ambient shear flow

Results from three dimensional simulations of a sphere undergoing a step change in relative velocity, in a linear shear flow, are presented in this section. These results cover a range of *Re*. A dimensionless initial shear rate of $s_1 = 0.04$ will be used in all cases considered. Fig. 3(a)

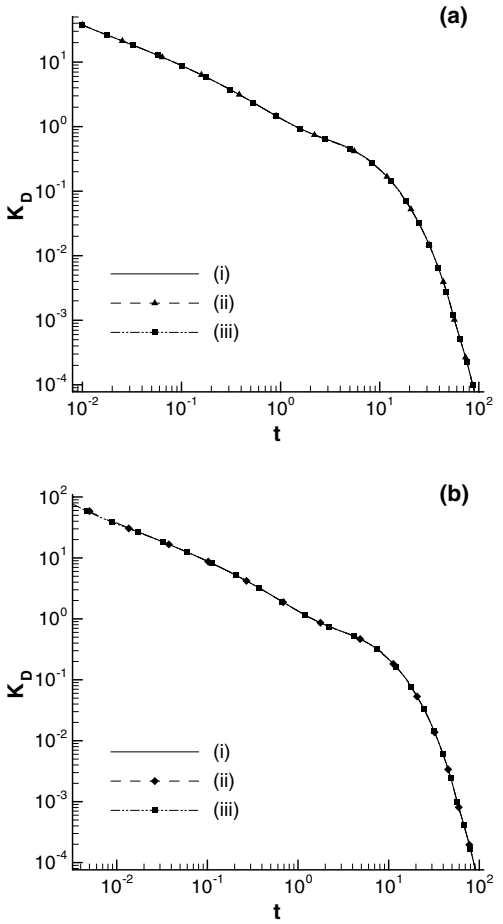

Fig. 2. Sensitivity of the history kernel to Δt and t_s for the same physical problem shown in Fig. 1. (a) Drag history kernel for the following three different cases: (i) $\Delta t = 1 \times 10^{-4}$ during rapid acceleration and later increased to 1×10^{-3}; (ii) Δt varied from 5×10^{-5} to 5×10^{-4}; (iii) Δt varied from 2.5×10^{-5} to 2.5×10^{-4}. (b) Drag history kernel for three different numerical approximations to delta function acceleration: (i) $t_s = 1 \times 10^{-2}$, (ii) $t_s = 5 \times 10^{-3}$ and (iii) $t_s = 2.5 \times 10^{-3}$.

compares the drag history kernels obtained from four different shear flow simulations with that obtained from a uniform ambient flow (shown earlier in Fig. 1). In all four shear flow cases considered, the relative velocity between the particle and the local undisturbed ambient flow was held constant for $t < 0$ and the relative velocity was linearly varied (over a short period) to the final relative velocity, which was held steady for $t > t_s$. The four different cases differ only in their initial and final Reynolds numbers and they are (i) $Re_1 = 5$, $Re_2 = 6.25$; (ii) $Re_1 = 50$, $Re_2 = 62.5$; (iii) $Re_1 = 62.5$, $Re_2 = 50$; and (iv) $Re_1 = 100$, $Re_2 = 125$.

The comparison clearly shows that at the present magnitude, there is very little influence of ambient shear on the drag history kernel, provided that the initial and final states of relative velocity are maintained the same. In all the cases considered, the short-term decay goes as $t^{-1/2}$.

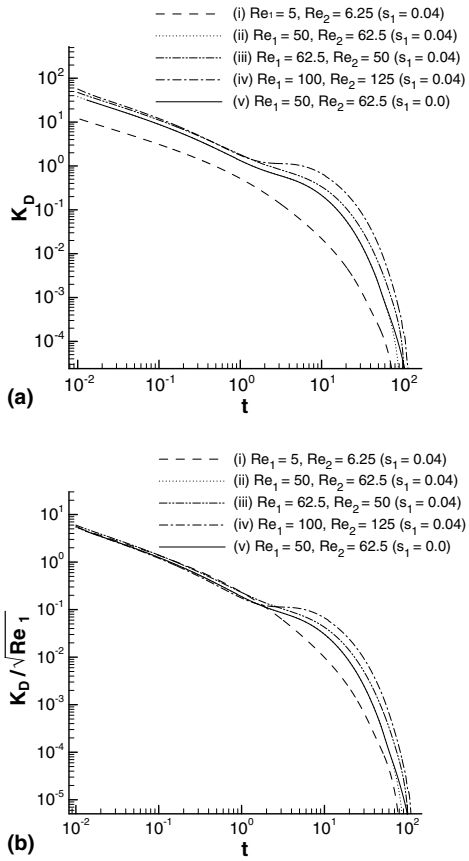

Fig. 3. (a) A comparison of the drag history kernels for the following cases: (i) ambient shear flow $Re_1 = 5$, $Re_2 = 6.25$; (ii) ambient shear flow $Re_1 = 50$, $Re_2 = 62.5$; (iii) ambient shear flow $Re_1 = 62.5$, $Re_2 = 50$; (iv) ambient shear flow $Re_1 = 100$, $Re_2 = 125$; and (v) ambient uniform flow $Re_1 = 50$, $Re_2 = 62.5$. (b) A plot of $K_D/\sqrt{Re_1}$ versus t for all the cases shown (a). The results for case (v) are virtually on top of those of case (ii).

Furthermore, the drag kernels for $t < 1$ for the different cases can be well collapsed when scaled as $K_D/\sqrt{Re_1}$. These time and Reynolds number scalings are consistent with the low Re analytic behavior described in the Boussinesq–Basset kernel. The figure also illustrates the expected long-time dependency of the history kernel on the nature of acceleration and on the start and end conditions. For example, when relative velocity was accelerated from $Re_1 = 50$ to $Re_2 = 62.5$, the pre-existing wake was strengthened, while when relative velocity was decelerated from $Re_1 = 62.5$ to $Re_2 = 50$, the pre-existing stronger wake was weakened. The difference in history kernel between these two cases is attributable to the above-mentioned difference in the wake processes. See the paper by Lovalenti and Brady (1993b) and Appendix D by E.J. Hinch, for a discussion of the wake effect on the history kernel in the limit of small Reynolds numbers. The effect of non-linearity in terms of both finite particle Reynolds number as well as the finite change between start and end conditions is evident.

3.3. Lift history kernel

The time evolution of lift force for the four different cases: (i) $Re_1 = 5$ to $Re_2 = 6.25$, (ii) $Re_1 = 50$ to $Re_2 = 62.5$, (iii) $Re_1 = 62.5$ to $Re_2 = 50$ and (iv) $Re_1 = 100$ to $Re_2 = 125$ are shown in Fig. 4(a). In all four cases, the initial non-dimensional shear rate was set at $s_1 = 0.04$. The steady state lift coefficient at $Re_1 = 5$ is 4.05×10^{-3}. The immediate effect of rapid increase in relative velocity, over the short-time span, appears as the sudden increase in lift coefficient to a value of about 6.6×10^{-3}. Subsequently, the lift coefficient shows a slow evolution and approaches the final steady state value of 2.78×10^{-3} corresponding to $Re_2 = 6.25$. The behavior for the other cases considered is similar—there is a rapid change in lift coefficient during acceleration, followed by a slow evolution to the final steady state. For example, in case (iv), since the Reynolds numbers ($Re_1 = 100$ and $Re_2 = 125$) are large, the quasi-steady lift coefficients before and long after the end of acceleration are negative (Kurose and Komori, 1999). The immediate effect of acceleration is a rapid positive jump in lift coefficient and as a result, for a short duration following acceleration, the lift coefficient becomes slightly positive, before decaying slowly to its final steady state value of

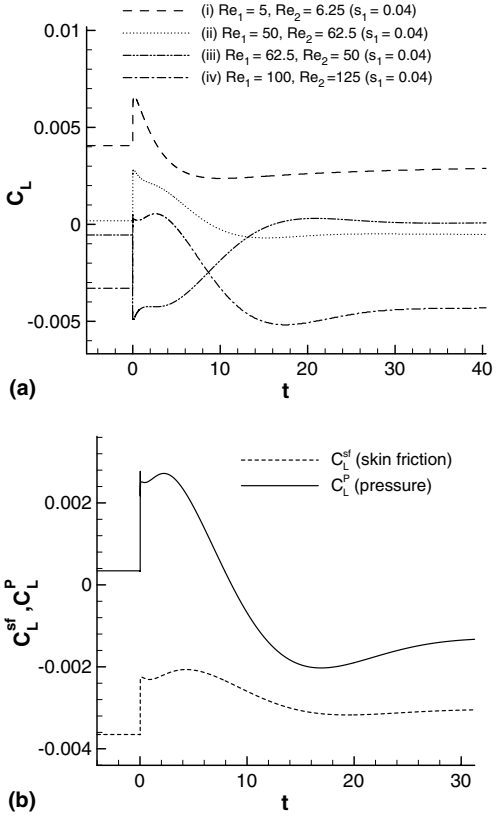

Fig. 4. (a) Time evolution of lift coefficient in an ambient shear flow with $s_1 = 0.04$, for the following cases: (i) $Re_1 = 5$, $Re_2 = 6.25$; (ii) $Re_1 = 50$, $Re_2 = 62.5$; (iii) $Re_1 = 62.5$, $Re_2 = 50$; and (iv) $Re_1 = 100$, $Re_2 = 125$. (b) Time evolution of the skin friction and pressure components of the lift coefficient corresponding to case (iv): $Re_1 = 100$, $Re_2 = 125$.

-4.34×10^{-3}. For case (iii), where relative velocity is decelerated from $Re_1 = 62.5$ to $Re_2 = 50$, the rapid change in C_L immediately following the deceleration is negative.

The non-monotonic approach to the final steady state seen in Fig. 4(a) is consistent with earlier results of Bagchi and Balachandar (2002a). During the post-acceleration phase, contributions to lift force from the added-mass and pressure-gradient effects are zero and as a result the non-monotonic approach to final steady state is due to the history effect. The multiple local peaks and valleys most clearly seen in the higher Reynolds number case is suggestive of an oscillatory approach to the final steady state. Fig. 4(b) shows the time evolution of the pressure and skin friction components of the lift force for case (iv). It is clear that the effect of sudden acceleration is manifested both in the pressure and skin friction contributions. Furthermore, the oscillatory nature of the lift force subsequent to rapid acceleration is seen in both contributions.

Fig. 5(a) shows the lift history kernel extracted from the lift coefficients shown in Fig. 4(a) using (11). The history kernel corresponding to the low Re asymptotic result of Asmolov and McLaughlin (1999) (discussed below) is also shown. The drag kernel exhibits a $t^{-1/2}$ short-time behavior and as a result blows up as $t \to 0$. In contrast, the lift kernel seems to approach a constant value as $t \to 0$, which seems to be different for the different cases considered and thus shows a Reynolds number dependence. In all cases for very short time, the lift kernel slightly increases with time. Thus, only for t greater than about 5 the amplitude of lift kernel begins to decay rapidly. These behaviors are qualitatively consistent with the results of Asmolov and McLaughlin (1999).

As seen in Fig. 3(b) the drag history kernel scales as $\sqrt{Re}$. The same scaling, however, does not collapse the lift history kernel. In Fig. 5(b) the lift history kernel is plotted as K_L/Re_G versus time and a good collapse of the different cases can be seen, suggesting a linear scaling of K_L with Re (note that $Re_G = sRe$). Fig. 5(b) shows an expanded view of the lift history kernel for short times plotted on a linear-log scale. This fundamentally different Reynolds number scaling for the drag and lift history forces will be addressed below. It is also evident that the lift history kernel is non-monotonic and takes on both positive and negative values. The level of oscillation tends to increase with Reynolds number. The difference between the four cases illustrates the dependence of the lift history kernel on the nature of acceleration and on the start and end conditions. This complex dependence for lift is consistent with the corresponding behavior observed in the drag history kernel.

The lift history kernel appears to be a superposition of a positive monotonic part and an oscillatory contribution in time. The amplitude of the oscillatory part is of sufficient strength that the lift kernel becomes negative at intermediate times. The decay of the kernel is quite rapid and as a result it is hard to fully discern the oscillatory behavior. A careful zoom-up of the kernel as it reaches very small values confirms the oscillatory nature of the kernel.

The above feature of the lift kernel is not entirely different from that of the drag. A close look at the drag kernel in Fig. 3 shows that its behavior is not inconsistent with the presence of an oscillatory component. In particular, the hump that is seen in the present results at $t \approx 10$ (which was also observed in the results of Mei (1993)) is similar to the more pronounced peak observed in the lift kernel. In the drag kernel, the relative strength of the oscillatory part is not strong enough, perhaps, to result in negative values at intermediate times. An interesting point to note is that the hump in the drag kernel is present even in a uniform flow and is observed only at finite Re. The hump is distinctly absent in the corresponding low Re asymptotic results. Thus, the oscillatory behavior seen in lift is a finite Reynolds number effect as well.

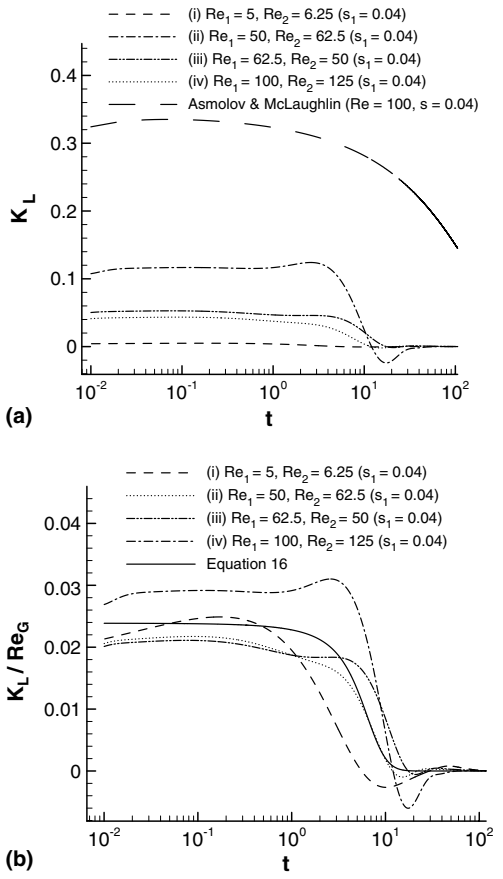

Fig. 5. (a) A comparison of the lift history kernels for the following cases (with dimensionless shear rate $s_1 = 0.04$): (i) $Re_1 = 5$, $Re_2 = 6.25$; (ii) $Re_1 = 50$, $Re_2 = 62.5$; (iii) $Re_1 = 62.5$, $Re_2 = 50$; (iv) $Re_1 = 100$, $Re_2 = 125$; and the Asmolov and McLaughlin (1999) result at $Re = 100$. (b) A plot of K_L/Re_G versus t for cases (i)–(iv) shown in (a). Also plotted is a simple curve fit through the computational data. Note that (ii) presents a case of acceleration and (iii) is the corresponding deceleration case. The difference between the two illustrates the role of a pre-existing wake on the kernel.

4. Discussion

The transient component of lift force can be theoretically analyzed in both inviscid and low Re limits. Asmolov and McLaughlin (1999) considered a sphere undergoing small amplitude streamwise oscillation in a linear shear flow, in the limit $Re \ll Re_G^{1/2} \ll 1$, and obtained an expression for time-dependent lift force in the frequency domain. Their expression for lift force can be written as

$$\tilde{F}_L^* = (9/4\pi)\rho d^2 \tilde{u}_r^*(G^*\nu)^{1/2}(2.254 + J'(\omega^*/G^*)), \tag{12}$$

where tilde represents the Fourier coefficient. The time-dependent relative velocity and corresponding lift force are $u_r^*(t^*) = \tilde{u}_r^* \exp[-\imath\omega^* t^*]$ and $F_L(t^*) = \tilde{F}_L^* \exp[-\imath\omega^* t^*]$, where ω^* is the dimensional frequency of oscillation. In the above equation the constant on the right hand side, 2.254, accounts for the quasi-steady lift force (or the Saffman lift force), which depends only

on instantaneous relative velocity between the particle and the ambient flow. The second term accounts for the history effect in lift force.

From definition (5) it can be seen that both the quasi-steady and history contributions to lift coefficient obtained from (12) scale as $\sqrt{s}/\sqrt{Re}$. This translates to the following scaling for the lift kernel: $K_L \propto \sqrt{sRe}$. In the case of drag force, such low Re asymptotic scaling (i.e., $K_D \propto \sqrt{Re}$) was observed to be appropriate even at finite Re, provided attention was restricted to small times (see Fig. 3). In contrast, in Fig. 5(b), it can be seen that the lift history kernels for the different Reynolds number cases collapse reasonably when normalized as K_L/sRe. It is thus clear that the observed behavior of the computed unsteady lift force departs from the low Re prediction.

The conditions of present simulations differ from those of Asmolov and McLaughlin (1999) in several significant ways. In addition to low Re and small amplitude limits, their analysis was restricted to the case of a sinusoidally oscillating sphere, whose mean motion (and mean Re) was zero. Furthermore, the additional restriction of asymptotically strong shear ($Re \ll Re_G^{1/2}$) employed in their analysis is clearly not applicable in the present simulations. These differences contribute to the disagreement seen in Fig. 5 between the computed lift history kernels and the corresponding prediction based on the analysis of Asmolov and McLaughlin (1999).

We will now turn to the inviscid limit to draw support for the present finite Re behavior. Lift force on a clean spherical bubble, suddenly introduced into a linear shear flow, has been considered by Legendre and Magnaudet (1998). They argued that immediately following acceleration (or introduction of the bubble) an irrotational velocity perturbation that satisfies the no-penetration condition on the bubble establishes. On a short-time scale, the redistribution of ambient vorticity by the irrotationally perturbed flow results in a lift force of $(\pi/8)\rho d^3 G^* u_r^*$. This result can be compared against the steady state lift force for an inviscid flow under the same configuration. In the limit of weak vorticity, Auton (1987) showed the steady state lift force on a sphere immersed in an ambient linear shear flow to be $(\pi/12)\rho d^3 G^* u_r^*$. Thus, in the inviscid limit, in a linear shear flow the lift coefficient on a sphere (as defined in (5)) starts from s immediately after introduction and decreases to an asymptotic steady state value of $2s/3$ (here s corresponds to the final state). Legendre and Magnaudet (1998) explained this inviscid temporal variation to be due to vorticity advection.

Using (11), the above inviscid result for the lift force can be re-casted into the following expression for the lift history kernel:

$$K_{L,\mathrm{invis}}(t \to 0+) = \frac{Re}{24}\left(C_L(t \to 0+) - C_L(\infty)\right) = \frac{Re_G}{72} = \frac{sRe}{72}. \tag{13}$$

The scaling $K_L \propto Re$ observed in the present finite Re computations is in agreement with the above inviscid prediction. Furthermore, the above-predicted linear dependence of the lift kernel on the ambient non-dimensional shear rate is distinctly different from the low Re prediction of $K_L \propto \sqrt{s}$. In order to test the validity of the above inviscid prediction ($K_L \propto s$) at finite Re, we performed an additional simulation for the $Re_1 = 100$, $Re_2 = 125$ case with a lower non-dimensional shear rate of $s_1 = 0.02$. The lift kernel obtained for this case is compared with that for the $s_1 = 0.04$ case in Fig. 6. When scaled by sRe, the kernels show a near perfect collapse, thus confirming the applicability of the inviscid scaling even at finite Re.

Legendre and Magnaudet (1998) numerically investigated the transient behavior at finite Re. At sufficiently large Re the theoretical predictions of the inviscid analysis were well recovered. Interestingly, even at $Re = 0.5$, where viscous effects can be expected to play a significant role, immediately

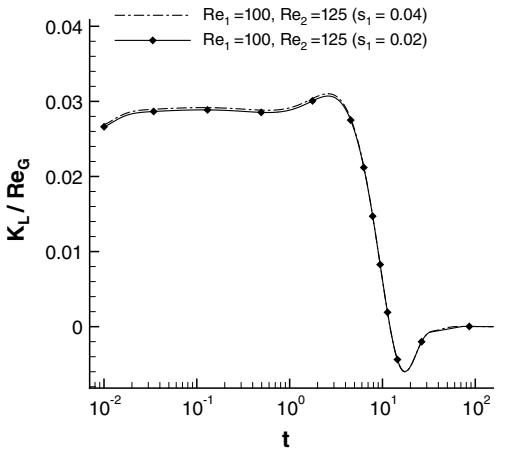

Fig. 6. Lift history kernel results for case (iv) of Fig. 5(a), plotted as K_L/Re_G for simulations performed at dimensionless shear magnitudes of $s_1 = 0.02$ and $s_1 = 0.04$.

following the acceleration the lift coefficient started at $C_L(t \to 0+) \to s$. However, the transient effect is now due to both advection and diffusion of vorticity, and the final steady state lift coefficient is different from the inviscid value of $2s/3$. The inviscid scaling can thus be expected to be relevant even at $O(1)$ Reynolds numbers and this provides additional support for the present results.

The results of Legendre and Magnaudet (1998) need to be properly adopted for quantitative comparison. First of all, their analysis was for a clean spherical bubble with a stress-free boundary condition on its surface. The present simulations are for a rigid sphere with a no-slip boundary. On a very short-time scale, the influence of rapid acceleration is dictated only by the inviscid perturbation induced by the sphere and as a result the inviscid analysis equally applies for a rigid sphere immediately following the acceleration. However, the difference between the two boundary conditions become quite clear in the final steady state. The steady state lift of a rigid sphere depends on both Reynolds number and non-dimensional shear, and the lift coefficient is quite small for Reynolds numbers greater than about 50 (Bagchi and Balachandar, 2002a; Kurose and Komori, 1999). In contrast, at large Reynolds numbers the lift coefficient of a clean bubble approaches $2s/3$. In other words, for the case of a rigid sphere we expect

$$C_L(t \to t_{s+}) \to s \quad \text{and} \quad C_L(\infty) \to \epsilon(Re, s), \tag{14}$$

where $\epsilon \approx 0$ for large Re.

Secondly, the problem considered by Legendre and Magnaudet (1998) is equivalent to accelerating the relative velocity between the bubble and the ambient shear flow from an initial stagnant state (i.e., $Re_1 = 0$) to a final steady state. In contrast, in all the simulations considered here, the acceleration followed an initial fully developed finite Re shear flow over the sphere. The dependence of history force on the details of such presence or absence of a pre-existing wake, prior to acceleration, has been well recognized in the context of drag (Lovalenti and Brady, 1993b). It is reasonable to expect such sensitivity in the detailed time evolution of the lift history force as well. Nevertheless, here we will apply the inviscid result of Legendre and Magnaudet (1998) for the present simulations, but now based on the incremental relative velocity due to acceleration.

That is, the factor $(Re_2 - Re_1)/Re_2$ will now premultiply the short-time lift coefficient given in (14). Based on this modification we obtain the following estimates

$$\begin{aligned} C_L(t \to t_{s+}) - C_L(\infty) &= \frac{s_2(Re_2 - Re_1)}{Re_2} - \epsilon(Re_2, s_2), \\ K_L(t \to 0+) &= \frac{Re_G}{24} - \frac{\epsilon Re_2^2}{24(Re_2 - Re_1)}. \end{aligned} \tag{15}$$

If we take ϵ to be zero then for the present simulations we obtain $K_L(t \to 0+)/Re_G \approx 0.04$. The value taken by the scaled kernels at short times, in Fig. 5(b), can be observed to be somewhat lower. The difference is perhaps due to the finite Re effect, and can be partially traced to the second term on the right hand side of (15).

Based on the observations above, here we propose the following simple expression for the lift history kernel:

$$K_L(t^*) = \frac{G^* d^2}{\nu}\left\{a_1\left[1 - \tanh\left(b_1\left[\frac{t^* u_r^*}{d}\right] - c_1\right)\right] + a_2\left[1 - \tanh\left(b_2\left[\frac{t^* u_r^*}{d}\right] - c_2\right)\right]\cos(\omega_2^* t^* + \phi_2)\right\}. \tag{16}$$

The first term on the right accounts for the non-oscillatory part and the second term accounts for the oscillatory component of the kernel. The coefficients, such as a_1, b_1 and c_1, can be expected to be weakly dependent on Reynolds number and the initial state of the flow before the start of acceleration. A reasonable fit for the range of cases considered in Fig. 5 can be obtained with $a_1 = 1.29 \times 10^{-2}$, $b_1 = 2.5 \times 10^{-1}$ and $c_1 = 1.27$. For lack of complete knowledge we do not attempt to model the oscillatory part.

We note that the history forces given in (6) and (10) for the drag and lift forces can be combined. This yields a second rank tensorial representation for the history kernel which will operate on the vectorial relative acceleration, $d\mathbf{u}_r^*/d\tau^*$. The diagonal entries of the history tensor will correspond to the drag kernel, while the off-diagonal entries will correspond to the lift kernel.

Finally, in Fig. 7, the flow field in the wake region behind the sphere is shown for case (iv) ($Re_1 = 100$, $Re_2 = 125$) at several time instances after acceleration has ended, where the lift kernel reaches local peak positive and negative values. These instances are marked in Fig. 7(a) as well. In frame (b), corresponding to the time instant before the start of the acceleration ($t < 0$), the flow field illustrates the steady state of the wake at $Re = 100$. Due to the presence of ambient shear, the wake structure is not axisymmetric. Shortly after acceleration, the recirculating zone in the wake is absent, as it is shed downstream due to the rapid acceleration of the ambient flow (see frames c and d). The flow around the sphere resembles that of an inviscid flow. Note that the ambient vorticity of the shear flow will be present and in fact this vorticity redistribution is the source of the rapid jump in lift force. This also conforms to the point made earlier that the lift force immediately following acceleration is primarily inviscid in origin. The recirculation region behind the sphere slowly forms on a longer viscous time scale after the end of acceleration (see frames e–g). Previous investigations (Bagchi and Balachandar, 2002c; Kurose and Komori, 1999) have clearly established that the wake vortical structure plays a crucial role in determining the lift force at finite Re. Fig. 7 can be examined to see if the oscillatory lift force following the rapid acceleration is due to an oscillation in the wake structure. From the figure no such discernable wake oscillation can be observed. This is consistent with the earlier remark that such

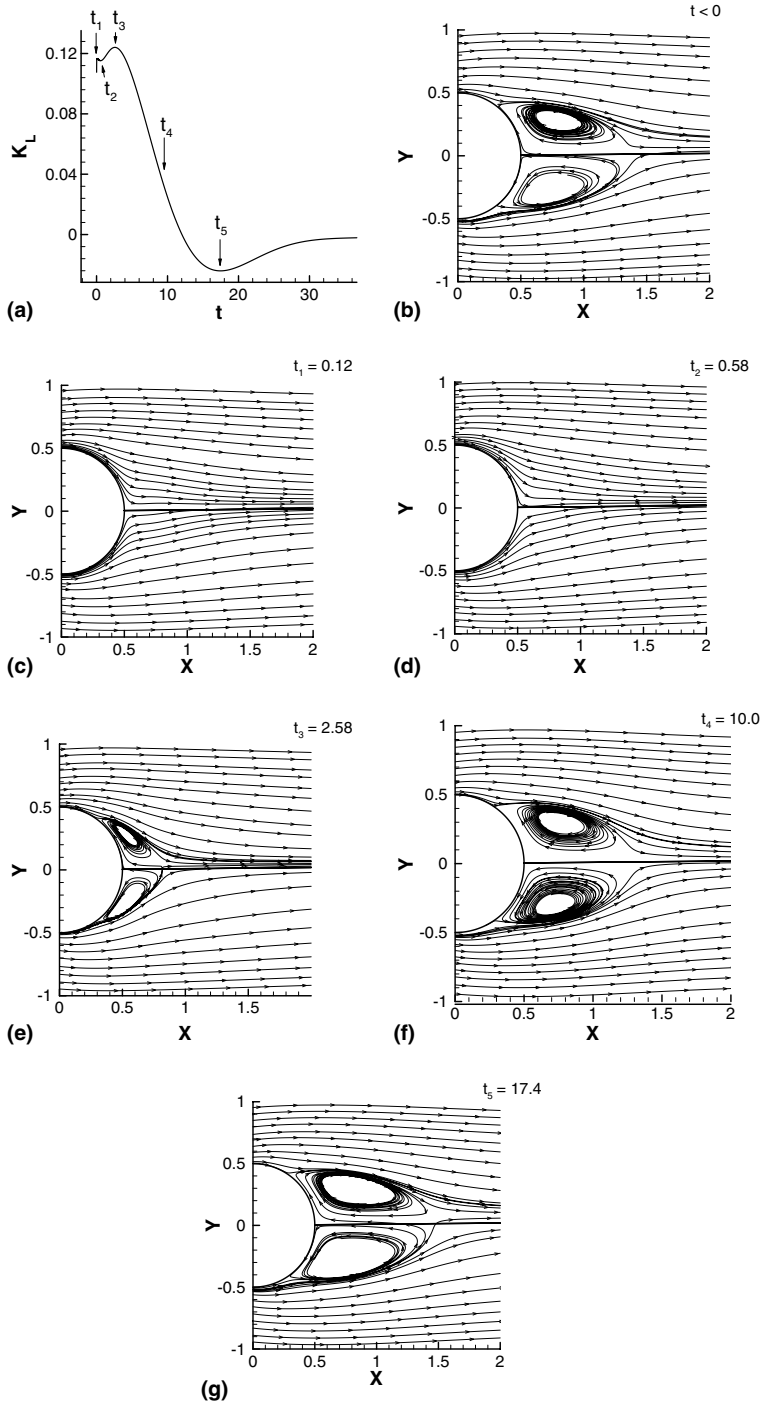

Fig. 7. (a) Lift kernel corresponding to a step change from $Re_1 = 100$ to $Re_2 = 125$, with a dimensionless ambient shear rate of $s_1 = 0.04$. The arrows indicate the time instances where the streamlines of the wake are visualized. (b) Fully developed wake streamlines at $Re_1 = 100$, before the step changes occurs ($t < 0$). (c)–(g) Streamlines of the wake at time instances corresponding to (a).

oscillations are present, perhaps, even in the absence of ambient shear, and are simply the result of finite Reynolds number. We also note that the oscillations are present even at $Re = 5$, where the recirculation region behind the sphere is clearly absent.

5. Conclusion

History forces on a spherical particle, due to rapid acceleration in a linear shear flow, are numerically investigated in this study. We consider simulations where the relative velocity of a spherical particle, in an unbounded linear shear flow, is rapidly changed from its initial to final value over a short period. Subsequent to this rapid acceleration, the relative velocity is maintained steady. Thus, from the drag and lift coefficients in the post-acceleration period, the corresponding drag and lift history kernel can be cleanly extracted. The ambient shear is found to have little effect on the drag history kernel. Furthermore, the drag kernel obtained in the present study is in agreement with that obtained by Mei (1993) in a similar study. In contrast, the lift history kernel shows an oscillatory behavior and hence the lift force approaches the final steady state in a non-monotonic way. As observed by other researchers (Mei, 1993; Lovalenti and Brady, 1993b) for the drag kernel, here we find the lift kernel to exhibit strong dependence on the nature of acceleration and on the start and end conditions.

Low Re asymptotic analysis of Asmolov and McLaughlin (1999) suggests a $\sqrt{sRe}$ scaling for the lift kernel, which is comparable to the corresponding $\sqrt{Re}$ scaling for the drag kernel. While the drag kernel obtained from the finite Re simulations follow the low Reynolds number analytic behavior quite well at small time, the corresponding lift kernel appears to deviate from the asymptotic behavior even at small times. The computed lift history kernel shows a linear scaling with Re. This fundamental difference in the scaling behavior of drag and lift history kernels arises from the inviscid origin of the lift force. For a sphere suddenly accelerated in a linear shear flow, Legendre and Magnaudet (1998) showed that the lift force immediately following the acceleration will be dictated by the advection of ambient vorticity by the inviscid perturbation field. Based on their result one can estimate the lift kernel to scale as $K_L \propto sRe$, and the present simulation results are in agreement with this prediction.

The important implication of the present result is that for a sphere undergoing relative acceleration with respect to an ambient shear flow, the instantaneous lift during and for a short while following the acceleration can be significantly different than the corresponding quasi-steady estimates. The quasi-steady lift coefficient for a particle is in general quite small even at modest Reynolds numbers. The lift force immediately after an acceleration however follows the inviscid prediction and therefore can be substantially larger. Thus, the unsteady component of lift can become important under appropriate conditions.

Acknowledgements

This research is supported by the ASCI Center for the Simulation of Advanced Rockets at the University of Illinois at Urbana-Champaign through the US Department of Energy (subcontract number B341494). The National Center for Supercomputing Applications (UIUC) is also

acknowledged, for the use of their computational facilities. The authors would also like to express their appreciation to Professors Prosenjit Bagchi and John B. McLaughlin, for their assistance and insightful comments.

Appendix A. Kernel extraction appendix

The infinite particle acceleration at $t^* = 0$ was approximated numerically as follows:

$$\frac{\mathrm{d}u_r^*(t^*)}{\mathrm{d}t^*} = \frac{\Delta u_r}{t_s^*}[H(t^*) - H(t^* - t_s^*)], \tag{A.1}$$

where t_s^* is the length of time over-which the acceleration is applied and $H(t^*)$ is a Heaviside function defined as

$$H(t^*) = \begin{cases} 1, & t^* > 0, \\ 0, & t^* < 0. \end{cases} \tag{A.2}$$

Let $f^*(t^*)$ represents the integral in the history term, with the approximated acceleration:

$$f^*(t^*) = \int_0^{t^*} K_{\mathrm{D}}(t^* - \tau^*) \frac{\Delta u_r^*}{t_s^*}[H(\tau^*) - H(\tau^* - t_s^*)]\,\mathrm{d}\tau^*. \tag{A.3}$$

Based on Eq. (6), this implies that, for $t^* > 0$,

$$f^*(t^*) = \frac{1}{3\pi\mu d}[F^*(t^*) - F_{\mathrm{QS}}^*(t^*)], \tag{A.4}$$

or, in non-dimensional terms (with u_{r1}^* as the velocity scale),

$$f(t) = \frac{u_{r2} Re_2}{24}[C_{\mathrm{D}}(t) - C_{\mathrm{D}}(\infty)]. \tag{A.5}$$

If we let $t - \tau = \xi$, then Eq. (A.3) becomes

$$f(t) = \frac{\Delta u_r}{t_s} \int_{t-t_s}^{t} K_{\mathrm{D}}(\xi)\,\mathrm{d}\xi. \tag{A.6}$$

Thus, for $t_s \ll 1$

$$f(t) \approx \Delta u_r \int_0^t K_{\mathrm{D}}(t - \tau)\delta\left(\tau - \frac{t_s}{2}\right)\mathrm{d}\tau. \tag{A.7}$$

This yields

$$K_{\mathrm{D}}\left(t - \frac{t_s}{2}\right) \approx \frac{1}{\Delta u_r} f(t). \tag{A.8}$$

The change of variables $t' = t - \frac{t_s}{2}$ finally yields the following expression (in terms of Re_1 and Re_2):

$$K_{\mathrm{D}}(t') \approx \frac{Re_2^2}{24(Re_2 - Re_1)}\left[C_{\mathrm{D}}\left(t' + \frac{t_s}{2}\right) - C_{\mathrm{D}}(\infty)\right]. \tag{A.9}$$

Since (A.9) is only valid after the acceleration, it follows that $t' > \frac{t_s}{2}$.

References

Asmolov, E., McLaughlin, J., 1999. The inertial lift on an oscillating sphere in a linear shear flow. Int. J. Multiphase Flow 25, 739–751.

Auton, T., 1987. The lift force on a spherical body in a rotational flow. J. Fluid Mech. 183, 199–218.

Bagchi, P., Balachandar, S., 2002a. Effect of free rotation on the motion of a solid sphere in a linear shear flow at moderate Reynolds number. Phys. Fluids 14, 2719–2737.

Bagchi, P., Balachandar, S., 2002b. Shear versus vortex-induced lift force on a rigid sphere at moderate *Re*. J. Fluid Mech. 473, 379–388.

Bagchi, P., Balachandar, S., 2002c. Steady planar straining flow past a rigid sphere at moderate Reynolds number. J. Fluid Mech. 466, 365–407.

Basset, A., 1888. A Treatise on Hydrodynamics. Dover, London.

Boussinesq, J., 1885Sur la Résistance Qu'oppose un Fluide Indéfini au Repos, Sans Pesanteur au Mouvement Variédùne Sphere Solide quìl Mouille sur Toute sa Surface, Quand les Vitesses Restent bien Continues et Assez Faibles por que Leurs Carrés et Produits Soient Négligeables, vol. 100. C.R. Academic Science, Paris, p. 935.

Chang, E., Maxey, M., 1994. Accelerated motion of rigid spheres in unsteady flow at low to moderate Reynolds numbers. Part 1. Oscillatory motion. J. Fluid Mech. 277, 347–379.

Chang, E., Maxey, M., 1995. Unsteady flow about a sphere at low to moderate Reynolds number. Part 2. Accelerated motion. J. Fluid Mech. 303, 133–153.

Kim, I., Elghobashi, S., Sirignano, W., 1998. On the equation for spherical particle motion: effect of Reynolds and acceleration numbers. J. Fluid Mech. 367, 221–253.

Kurose, R., Komori, S., 1999. Drag and lift forces on a rotating sphere is a linear shear flow. J. Fluid Mech. 384, 183–206.

Landau, L., Lifshitz, E., 1959. Course of Theoretical Physics Fluid Mechanics, vol. 6. Pergamon, Oxford.

Lawrence, C., Mei, R., 1995. Long-time behavior of the drag on a body in impulsive motion. J. Fluid Mech. 283, 307–327.

Legendre, D., Magnaudet, J., 1998. The lift force on a spherical bubble in a viscous linear shear flow. J. Fluid Mech. 368, 81–126.

Lovalenti, P., Brady, J., 1993a. The force on a sphere in a uniform flow with small amplitude oscillations at finite Reynolds number. J. Fluid Mech. 256, 607–614.

Lovalenti, P., Brady, J., 1993b. The hydrodynamic force on a rigid particle undergoing arbitrary time-dependant motion at small Reynolds number. J. Fluid Mech. 256, 561–605.

Lovalenti, P., Brady, J., 1995. The temporal behavior of the hydrodynamic force on a body in response to an abrupt change in velocity at small but finite Reynolds number. J. Fluid Mech. 293, 33–46.

Mei, R., 1993. History force on a sphere due to a step change in the free-stream velocity. Int. J. Multiphase Flow 19, 509–525.

Mei, R., 1994. Flow due to an oscillating sphere and an expression for unsteady drag on the sphere at finite Reynolds number. J. Fluid Mech. 270, 133–174.

Mei, R., Adrian, R., 1992. Flow past a sphere with an oscillation in the free-stream velocity and unsteady drag at finite Reynolds number. J. Fluid Mech. 237, 323–341.

Mei, R., Lawrence, C., Adrian, R., 1991. Unsteady drag on a sphere at finite Reynolds number with small fluctuations in the free-stream velocity. J. Fluid Mech. 233, 613–631.

Michaelides, E., 1997. Review—the transient equation of motion for particles, bubble and drops. J. Fluids Eng. 119, 233–247.

Mittal, R., Balachandar, S., 1996. Direct numerical simulation of flow past elliptic cylinders. J. Comp. Phys. 124, 351.

Miyazaki, K., Bedeaux, D., Bonet, A., 1995. Drag on a sphere in a slow shear flow. J. Fluid Mech. 296, 373–390.

Sano, T., 1981. Unsteady flow past a sphere at low Reynolds number. J. Fluid Mech. 112, 433–441.

Stokes, G., 1851. On the effect of internal friction of fluids on the motion of pendulum. Trans. Camb. Philos. Soc. 9, 8–27.